Vessel-based brain-shift compensation using elastic registration driven by a patient-specific finite element model

Fanny Morin, Ingerid Reinertsen, Hadrien Courtecuisse, Olivier Palombi,
Bodil Munkvold, Hans Kristian Bø, Yohan Payan, Matthieu Chabanas

HAL Id: hal-01331713
https://hal.archives-ouvertes.fr/hal-01331713

Submitted on 14 Jun 2016

Vessel-based brain-shift compensation using elastic registration driven by a patient-specific finite element model

**Fanny Morin · Ingerid Reinertsen ·
Hadrien Courtecuisse · Olivier Palombi ·
Bodil Munkvold · Hans Kristian Bø ·
Yohan Payan · Matthieu Chabanas**

Abstract *Purpose* The purpose of this paper is to provide a proof of concept of a new brain-shift compensation method. During brain tumor surgery, planning and guidance are based on pre-operative images which do not account for brain-shift. However, this deformation is a major source of error in neuro-navigation systems and affects the accuracy of the procedure.
Methods A patient-specific biomechanical model accounting for blood vessels around the tumor and brain soft tissues is built from the pre-operative images. Intra-operatively, the vascular tree is extracted from Doppler ultrasound acquisitions and registered to the pre-operative one using the biomechanical model. The deformations are thus extrapolated from the blood vessels to the surrounding soft tissues in order to update the pre-operative images.
Results Quantitative and qualitative results on a single surgical case are provided, with an evaluation of the execution time for each processing step. The average brain-shift measured on blood vessels is reduced from 3.98 mm to 1.38 mm with our method against 2.59 mm with the closest pure image registration algorithm in the literature. In addition, the registration of the tumor is significantly increased.
Conclusions In this paper, a proof of concept of a new gravity-induced brain-shift compensation technique is presented. This method is proved to be efficient to compensate for brain deformation while being compatible with a surgical process.

F. Morin (✉ fanny.morin@imag.fr) · Y. Payan · M. Chabanas
TIMC-IMAG, Univ. Grenoble Alpes, CNRS, F-38000 Grenoble, France

F. Morin · H. Courtecuisse
AVR-ICube, Univ. Strasbourg, CNRS, Strasbourg, France

I. Reinertsen
SINTEF, Dept. Medical Technology, Trondheim, Norway

B. Munkold · H. K. Bø
St. Olav University Hospital (NTNU), Dept. of Neurosurgery, Trondheim, Norway

O. Palombi
Grenoble University Hospital, Dept. of Neurosurgery, F-38000 Grenoble, France

1 Introduction

Accurate localization of brain tumor is essential to both ensure its total resection and reduce the morbidity of surrounding healthy tissues. However, the intra-operative deformation of soft tissues, called "brain-shift", affects this localization. Reporting cortical surface displacements ranging up to 24 mm, [13] observed that the brain-shift is influenced by several parameters: tissue characteristics, size and location of the craniotomy, loss of cerebro-spinal fluid (CSF) and resected volume.

Using a biomechanical model to compensate for this non-linear deformation requires complex parametrization in terms of biomechanical properties (constitutive laws and parameters) and boundary conditions [10]. In addition, these input parameters are dependent on the patient and phenomena preceding the procedure (e.g. X-ray treatment). Thus, biomechanical models alone struggle to accurately predict the deformation without further information.

As high contrast information about the soft tissues are provided by Magnetic Resonance Imaging (MRI), this is the reference pre-operative imaging for brain surgeries. [22] thus proposed to register pre-operative MRI to intra-operative MR acquisitions using a biomechanical model. However, due to their cost, such MR scanners are available in very few operating rooms. This intra-operative imaging technique is thus rarely used in clinical routine.

Several acquisitions of the cortical surface can be performed during surgery using a laser-range scanner [5,8] or a stereo-camera [20]. The brain 3D deformations are then recovered using a surface registration algorithm combined with an atlas of the soft tissues deformations computed pre-operatively. These methods thus make the strong assumption that all the 3D deformations can be extrapolated from the exposed surface of the brain. However, according [25], the registration accuracy improves when data are collected from both the exposed and unexposed surface of the brain.

In the literature, some pure image-to-image registration methods relying on intra-operative ultrasound (US) acquisitions are also proposed. An US scanner has the benefit to cost less than 10% of a MR scanner. It is portable, compatible with other surgical equipment and available in most operating theaters. However, the US imaging suffers from poor image quality explaining its limited expansion in neuro-navigation systems. Intra-operative B-mode US imaging enables to visualize tissues close to the tumor region. [17] presented a method to register pre-operative MRI to intra-operative B-mode US images. Nevertheless, MRI and US imaging rely on very different physical principles and then various image characteristics (intensity, noise, contrast, volume coverage, etc). Their registration is thus a challenging problem. Doppler US imaging provides flows visualization (e.g. the vascular tree). [14,16] proposed a modified Iterative Closest Point (ICP) algorithm and a non-linear transformation using thin-plate spline to register blood vessels from pre-operative MR angiography (MRA) onto intra-operative Doppler US acquisition. The brain-shift compensation using rigid registration was validated with clinical study on 7 patients in [15]. However, such a method has limits since brain-shift deformation cannot only be approximated by a rigid transformation.

In this paper, a new method for gravity-induced brain-shift compensation is presented, based on the approach proposed by [15]. The blood vessels registration is then driven by a biomechanical patient-specific Finite Element (FE) brain model, in order to account for the non-linear behaviour of the organ as in [3]. In addition,
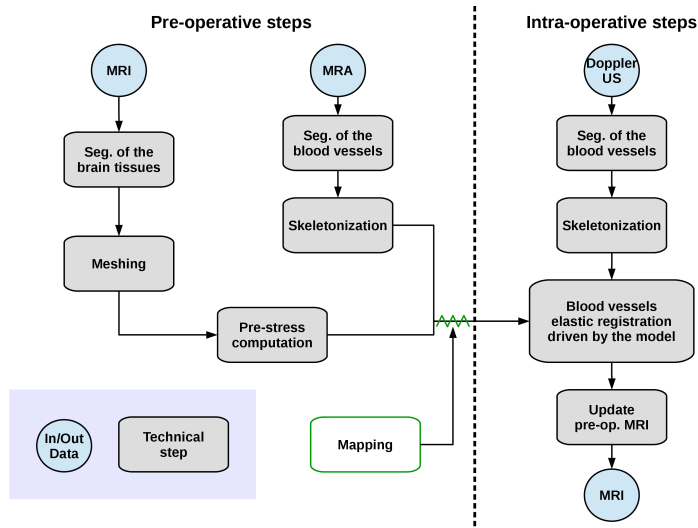
Fig. 1: Brain-shift compensation process

the method includes pre-operative and intra-operative processing steps compatible with a surgical process in term of execution time and user interactions.

2 Methods

The pipeline of our brain-shift correction method is detailed in Figure 1 :

- Pre-operatively, an anatomical patient-specific brain model is built from the pre-operative images, accounting for blood vessels around the tumor and brain soft tissues (see Section 2.1 for details).
- Intra-operatively, a 3D volume is reconstructed from 2D Power Doppler US slices. The vascular tree is then extracted in a fully automatic way and registered to the pre-operative one using the biomechanical model (see Section 2.2 for details).

The deformations of the vascular tree are thus extrapolated from the blood vessels to the tumor region. Results on a single clinical case are provided in Section 3, including the quantification of brain-shift compensation and the evaluation of execution times.

2.1 From pre-operative images to patient-specific model

2.1.1 Building of the soft tissues biomechanical model from MRI

Meshing: The cerebrum, cerebellum, brainstem and tumor are segmented from the pre-operative T1-MRI. The cerebrum and tumor are meshed with higher density of elements in the tumor area . The tentorium is identified as the border between the cerebrum and cerebellum. Since this membrane is quite rigid, the

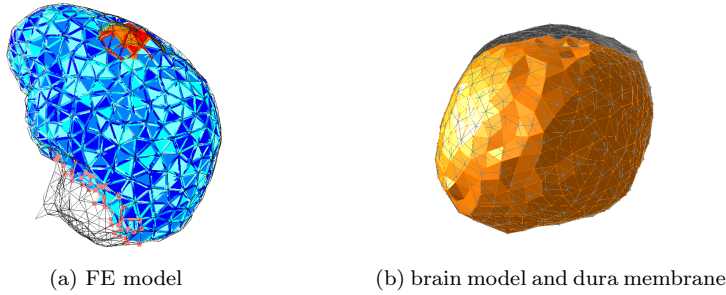(a) FE model   (b) brain model and dura membrane

Fig. 2: Patient-specific brain meshes

nodes located on the tentorium are fixed in the model (pink points on Figure 2
(a)). The dura is generated as the external surface of the brain FE mesh (in grey
on Figure 2 (b)) and assumed to be fixed throughout the simulation.

Constitutive law and parameters: As detailed in Section 2.2.2, imposed dis-
placements on vessels are used to drive the simulation. According to [9], the so-
lution in displacements in such simulation cases is weakly sensitive to the chosen
constitutive law and parameters. In addition, [24] advises to use a linear law un-
dergoing large displacements. The simulation of our model is thus handled with
the corotational approach proposed by [12]. Using this formulation, a linear law
with a non-linear geometric resolution is accounted for. Following [18], the Young's
modulus and Poisson's ratio are respectively set to 1.5 kPa and 0.45. A higher stiff-
ness equal to 10 kPa is used for the tumor. So far, these parameters are neither
patient-specific nor dependent on the type and location of the tumor.

Simulation: The dynamic equation is given by :

$$\mathbf{M}\ddot{\mathbf{q}} + \mathbf{B}\dot{\mathbf{q}} + \mathbb{F}(\mathbf{q}, \dot{\mathbf{q}}) + \mathbb{H}(\mathbf{q}, \mathbf{p}, \lambda) = 0 \tag{1}$$

where $\mathbb{F}(\mathbf{q}, \dot{\mathbf{q}})$ are the internal forces for the given positions $\mathbf{q}$ and velocities $\dot{\mathbf{q}}$. $\mathbf{M}$
and $\mathbf{B}$ are respectively the mass and the damping matrices. $\mathbb{H}(\mathbf{q}, \mathbf{p}, \lambda)$ gathers the
constraints forces λ for the current positions $\mathbf{q}$ and the targeted positions $\mathbf{p}$ (see
below). This formalism is here detailed to solve the contacts with the dura. It will
also be used in Section 2.2.2 during the blood vessels registration process.

The contacts between the cortex and the dura are solved using [7], inspired by
the ICP algorithm. At the beginning of each simulation step, each surface node
of the FE brain mesh (with position $\mathbf{q_i}$) is associated with a target position $\mathbf{p_i}$,
which is defined as the closest projection of $\mathbf{q_i}$ over the triangles of the dura mesh.
This association remains constant within a simulation step as in [6], allowing to
define the Jacobian of Constraints $\mathbf{J}$ and the violation of constraints δ. Sliding
constraints are used as in [7], allowing the brain to slide along the dura.

A Backward Euler implicit time integration is used for the simulation. This
yields to an augmented linear system :

$$\begin{cases} \mathbf{Ax} + \mathbf{J}\lambda = \mathbf{b} \\ \mathbf{A} = \frac{1}{h}\mathbf{M} + \mathbf{B} + h\frac{\partial \mathbb{F}}{\partial \mathbf{q}} \end{cases} \tag{2}$$

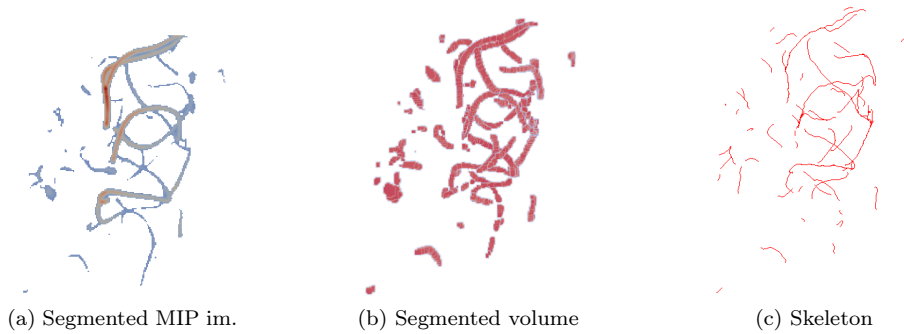(a) Segmented MIP im.   (b) Segmented volume   (c) Skeleton

Fig. 3: Blood vessels extraction from MRA

with $\mathbf{x}$ and $\mathbf{b}$, respectively the increment and residual in the Newton solver (see [6]). The schür complement method is used to solve system (2), involving the computation of the *compliance matrix* $\mathbf{W} = \mathbf{J}\mathbf{A}^{-1}\mathbf{J}^T$ that relates the mechanical coupling between constraints. After the resolution, λ is computed such that no positive violation δ remains between the dura surface and the brain.

Computation of gravity-induced internal stress: The brain shape segmented from the pre-operative MRI corresponds to an equilibrium state between internal and external forces. If the external forces are applied without accounting for the internal ones, an other equilibrium state will be reached, not corresponding anymore to the one segmented on the pre-operative data. Since internal forces are unknown, the external ones (e.g. the gravity) are most of the time ignored by the biomechanical models. As gravity is one of the main causes of the brain-shift, the gravity-induced internal pre-stress is computed using the algorithm detailed by [11] for a highly deformable model of the brain.

2.1.2 Blood vessels extraction from MRA

Segmentation: The blood vessels segmentation process is based on the Maximum of Intensity Projection (MIP) image analysis presented in [21]. After segmenting targeted vascular structures, the binarized MIP image is used as a mask to recover 3D positions of vessels into MRA 2D slices.

In order to get more contrast in the region of interest, the MRA is cropped to the tumor region before computing the MIP image. Two peaks are pointed out by the histogram of this resulting MIP image, respectively corresponding to the background and the soft tissues. The higher intensities then represent the blood vessels highlighted with a contrast product. The MIP image is thus segmented with a threshold set just after the second peak of the histogram (Figure 3 (a)).

Furthermore, artificial noise can appear due to the 3D reconstruction of the segmented volume. In order to increase robustness, the whole segmentation process is performed for the x, y and z directions of the 3D space, obtaining three segmentation volumes. Finally, the segmented vascular tree is computed as their intersection (Figure 3 (b)).
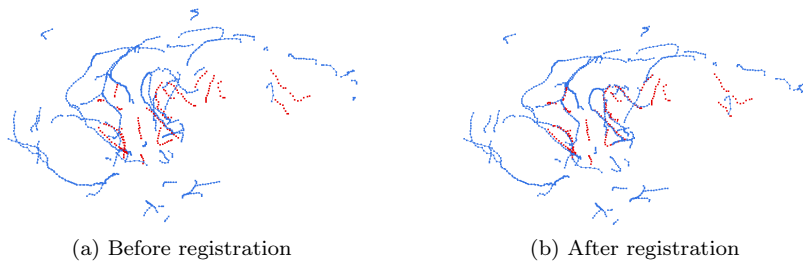
(a) Before registration   (b) After registration

Fig. 4: Elastic registration of MRA skeleton (blue) onto US skeleton (red)

Skeletonization: The blood vessels skeletonization process is based on the modified Dijkstra algorithm detailed in [23]. First, the Euclidian distance to the closest vessel boundary (DBF-distance) is computed for each voxel inside the vessels. The images are then converted into a connected graph, using the inverse value of the DBF-distance. Finally, the vascular branches are extracted using Dijkstra algorithm (Figure 3 (c)).

As the regularity of the extracted skeleton strongly depends on the quality and voxel's size of the input segmentation image, each branch is smoothed and re-sampled using B-splines. The number of points per millimeter is then uniformly set to 1 point/mm for the whole skeleton. Finally, points and their connectivity (segments) are exported and mapped into the FE brain model using barycentric coefficients.

2.2 Intra-operative elastic registration

2.2.1 Power Doppler US acquisition and blood vessels extraction

After opening of the skull, a series of 2D power Doppler US slices is acquired and reconstructed to a 3D volume using a Pixel Nearest Neighbour (PNN) algorithm. Such images provide high contrast information on the blood vessels and their segmentation is simply achieved by thresholding as in [14–16]. The skeletonization step is realised with the algorithm described in Section 2.1.2.

2.2.2 Elastic registration driven by patient-specific model

Elastic registration algorithm: The registration between the blood vessels extracted from the pre-operative MRA (source) and intra-operative Doppler US (target) is preformed following the formalism introduced in Section 2.1.1. At the beginning of each simulation step, the US target points, with positions $\mathbf{p}$, are associated with their respective nearest segment on the MRA skeleton. $\mathbf{q}$ is defined as the projection of $\mathbf{p}$ on the latter segments. Figure 4 illustrates the elastic registration between the MRA (blue) and US (red) skeletons.
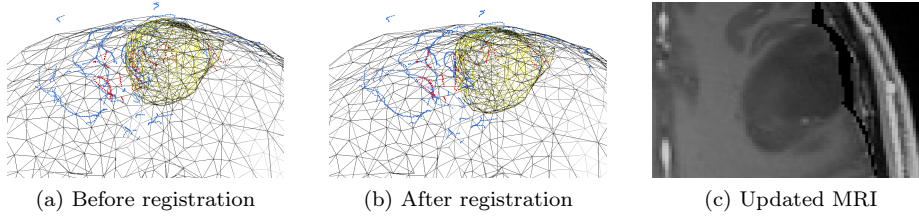
| (a) Before registration | (b) After registration | (c) Updated MRI |

Fig. 5: Update of pre-operative MRI using the biomechanical model

Filtering of the outliers: If the missing correspondences (e.g. the vessels along the direction of the US wave propagation) should be extrapolated by the biomechanical model, the inconsistent matching points have to be treated in order to make our elastic registration algorithm robust to the noise.

First, when a MRA segment matches several US points, only the nearest one is kept in order to avoid over-constrained situations. Moreover, an average amplitude and a principal direction of deformation were observed for the brain-shift. For each matching point, the distance $\delta_\mathbf{i}$ and the direction $\mathbf{n_i}$ are respectively defined as $\|\mathbf{p_i} - \mathbf{q_i}\|$ and $\mathbf{p_i} - \mathbf{q_i}$. These points are considered as outliers if one of the following conditions is not verified :

$$\begin{cases} \delta_i \in [\bar{\bar{\delta}} - \delta_t; \bar{\bar{\delta}} + \delta_t] \\ \mathbf{n_i}.\bar{\mathbf{n}} > -0.5 \end{cases} \tag{3}$$

where $\bar{\bar{\delta}}$ and $\bar{\mathbf{n}}$ are respectively the average distance and orientation and δ_t, a threshold set to 1mm.

Soft compliance factor: The constrained problem has a solution if and only if all the constraints are exactly verified at the end of each simulation step. However, deleting outliers is not sufficient to ensure that such a solution exists. To avoid oscillations at the end of the registration process, a soft compliance factor $\mathbf{W}^{soft}$ is added to the compliance matrix :

$$(\mathbf{W} + \mathbf{W}^{soft})\lambda - \delta = 0 \tag{4}$$

where $\mathbf{W}^{soft}$ is a diagonal matrix with coefficients uniformly set to c_{soft}.

Instead of deforming the MRA skeleton (and then the FE brain model), higher compliance allows US points to move if the necessary energy is too high to satisfy the constraint.

2.2.3 Update of pre-operative MRI

The pre-operative MRI is wrapped with the displacement field computed from the deformation of the FE mesh (Figure 5 (a), (b)) using barycentric coefficients. Figure 5 (c) shows the updated MRI in the region of the tumor.
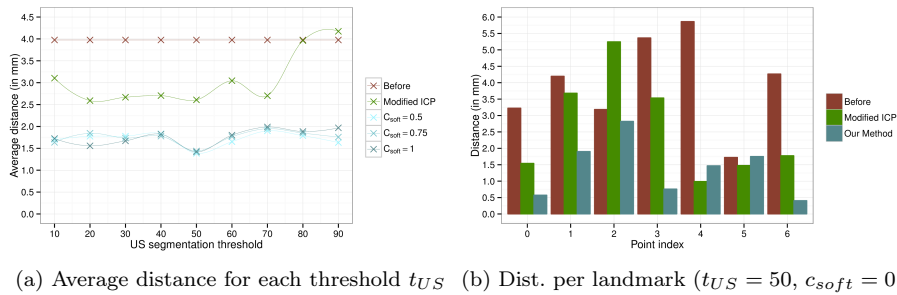
(a) Average distance for each threshold t_{US} (b) Dist. per landmark ($t_{US} = 50$, $c_{soft} = 0.5$)

Fig. 6: Quantitative results for blood vessels registration

3 Results

This section presents our results on one surgical case of low grade tumor located in the left frontal lobe. The data were collected by SINTEF Medical technology (Trondheim, Norway) using the navigation system CustusX [1].

Brain tissues were segmented from MR T1 images using ITK-SNAP [26]. Then, an FE mesh, composed of 3316 nodes and 16318 tetrahedral elements, was designed with CGAL (www.cgal.org). The patient-specific biomechanical model was developed using the simulation framework Sofa (www.sofa-framework.org). Finally, the MIP segmentation, the skeletonization and the update of the pre-operative MRI were implemented using the visualization framework Paraview [2] whereas the 3D reconstruction and the thresholding of intra-operative US images were handled by CustusX [1].

3.1 Brain-shift compensation results

Our non-rigid registration method was evaluated on the vascular tree and on the tumor region, and compared to the modified ICP of [14–16], available in CustusX [1]. In order to compare the registration processes only, all segmentation and skeletonization steps of the vascular tree were achieved with our method.

3.1.1 Blood vessels registration

Seven landmarks were manually identified on the blood vessels on both the pre-operative MRA and the intra-operative Power Doppler US images. The average distance between corresponding landmarks before and after registration is presented in Figure 6 (a) for several US segmentation thresholds (t_{US}) and 3 values of c_{soft} (see Section 2.2.2). As a first result and regardless of both parameters, better brain-shift compensation results are provided by our method.

For low US segmentation thresholds ($t_{US} < 40$), lot of noise is contained in the resulting skeletons and both registration methods seem quiet robust to this noise. However, when the value of this threshold increases ($t_{US} > 60$), the extracted vascular tree is incomplete. While our method seems robust to this loss of information, this is not the case for the modified ICP that finally diverges.

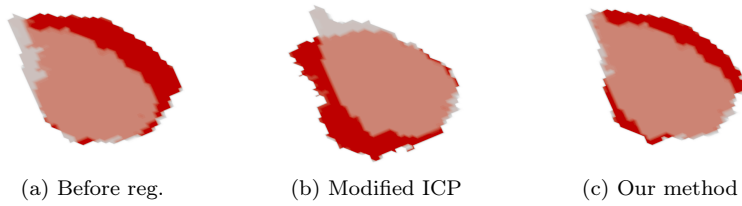(a) Before reg.   (b) Modified ICP   (c) Our method

Fig. 7: Registration results on a slice of MRI (in red) and US tumor (in light grey)

A good ratio between noise and loss of information is provided by fixing $t_{US} = 50$ and best registration scores are reached for both methods for this threshold. The distances between each respective landmark are shown for this threshold in Figure 6 (b). The landmark number 2 is located in a region that is not represented in the extracted skeletons. While our method barely diminishes the initial distance, the modified ICP significantly increases it, due to the rigid transformation.

Finally, the impact of c_{soft} on the registration results is low, especially for t_{US} close to 50 (Figure 6 (a)). However, this parameter is essential to reduce the oscillations and to make the method converge.

As a conclusion, the brain-shift measured on blood vessels (3.98 mm) is reduced on the best case to 1.38 mm with our method against 2.59 mm with the modified ICP. Furthermore, good brain-shift compensation results are obtained for large ranges of t_{US} and c_{soft}. This demonstrates the robustness of our method to the input data and parameters. For the next paragraphs, t_{US} and c_{soft} are respectively set to 50 and 0.5.

3.1.2 Tumor registration

In this section, the impact of the vessel-based compensation method on the tumor location is studied. The tumor was segmented on the pre-operative MRI and intra-operative B mode US by two medical experts from St Olav University Hospital (Trondheim, Norway). Both methods were applied on the MR segmentation : the modified ICP transformation matrix and the displacement field extracted from our FE model. Instead of comparing the outlines of the tumor, which can differ in MRI and B mode US, the registration score is computed as the 3D overlap of the segmented voxels (in %). Before registration, the US tumor is overlapped at 83.33% by the MRI tumor whereas after the rigid and our registration, this percentage is respectively equal to 84.52% and 93.27%.

The registration results are presented in Figure 7 on a slice of the tumor. For this patient, the extracted vascular tree is located under the tumor. The modified ICP slightly increases the overlap value and a leverage effect may appear due to the rigid transformation (rotation). With our method, the overlap value is higher thanks to the additional information contained in the biomechanical model.
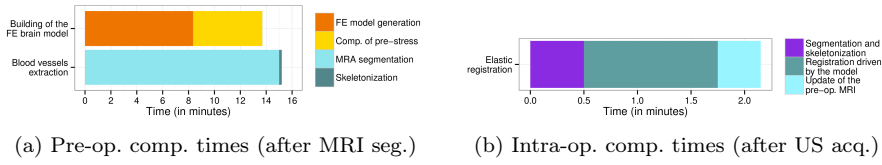
(a) Pre-op. comp. times (after MRI seg.)   (b) Intra-op. comp. times (after US acq.)

Fig. 8: Evaluation of the execution times

3.2 Integration to the surgical process

After showing the ability of our method to compensate for brain-shift on a single surgical case, its compatibility with a surgical process, in term of execution time, is studied in this section.

3.2.1 Model generation

Our method does not require a detailed brain tissues segmentation of the pre-operative MRI : only the envelops of the brain, cerebellum, brainstem and tumor are needed. For this clinical case, this segmentation was realised by an operator using ITK-SNAP [26] that is not a conceivable solution in a surgical process. However, this problem is fundamental in medical simulations and have been addressed several times in the literature. For example, [4] proposed an automatic method to warp an atlas mesh to fit the patient geometry described in a MRI data in a clinically relevant time scale. On an other hand, [19] presented a method to extract the brain surface within few seconds. In conclusion, some automated and time relevant solutions exist in the literature in order to segment the brain region, but have not yet been explored by the authors.

Our registration process have been tested with several FE brain mesh refinements between 1500 and 5000 nodes. The average distance between landmarks in blood vessels (for $t_{US} = 50$ and $c_{soft} = 0.5$) does not significantly change from one refinement to the other ($\pm$ 0.02mm). However, a too low number of nodes would yield to an over-constrained problem, especially for US skeletons with high noise. Thus, the size of our FE mesh was fixed around 3000 nodes which allows running the simulation in interactive time.

3.2.2 Evaluation of the execution times for each step

Figure 8, that presents execution times for pre-operative (a) and intra-operative steps (b), shows that our method is clinically time relevant. Before surgery, extracting the blood vessels and building the patient-specific FE model respectively from pre-operative MRA and MRI can be processed in parallel. Intra-operatively, [14–16] already showed that performing a Power Doppler US acquisition during surgery is time relevant. Furthermore, brain tumor surgeries last in general several hours and adding few more minutes (approximately 2 minutes for our whole registration process) to the procedure is acceptable.

4 Discussion and Conclusion

In this paper, a proof of concept of a new method was presented to compensate for brain-shift deformation, based on the registration of the vascular tree driven by a patient-specific FE model. Improvements over rigid registration of blood vessels [14–16] were quantified on a single surgical case. Moreover, our method is quasi-automatic, robust to the input data and parameters, executable in a relevant time scale, and thus compatible with a surgical process.

So far, results have been shown on a single case only and obviously have to be confirmed on other patients. For this purpose and in order to bring our system into a clinical environment, we aim to develop plug-ins to connect each step of our method to the navigation system CustusX [1], already used in current clinical studies.

Brain-shift compensation improvements over the modified ICP [14–16] were shown in Section 3.1. Furthermore, the recent clinical study presented in [8] over 16 patients reported a measured brain-shift (ranged from 2.5 to 21.3 mm before correction) after compensation between 0.7 and 4.0 mm. While these methods cannot be directly compared (different input data, validation,...), our results (1.38 mm after correction) seem consistent with the ones in [8].

However, several aspects of our method could be improved. First, image processing and registration parameters (segmentation, skeletonization, outliers treatment, etc.) should be automatically set based on the input data. Then, the biomechanical model can be enhanced, integrating further anatomical structures such as the dural septa [5] and the ventricles as well as the opening of the dura by the surgeon and the interactions between the soft tissues and the CSF. Moreover, the impact of the chosen constitutive law and parameters has to be quantified. Since these improvements might significantly increase the model complexity, the computations time could be reduced by GP/GPU parallelization, at least for the image processing steps. Finally, the tumor resection will have to be taken into account so that our brain-shift compensation method could be used not only at the opening of the skull but until the end of the surgery.

Compliance with ethical standards

Conflict of interest: The authors declare that they have no conflict of interest.

Ethical approval: For this type of study formal consent is not required.

Informed consent: Informed consent was obtained from all individual participants included in the study.

References

 1. Askeland, C., Solberg, O.V., Beate, J.B.L., Reinertsen, I., Tangen, G.A., Hofstad, E.F., Iversen, D.H., Vapenstad, C., Selbekk, T., Lango, T., Hernes, T.A., Leira, H.O., Unsgard, G., Lindseth, F.: CustusX: an open-source research platform for image-guided therapy. International journal of computer assisted radiology and surgery (2015)
 2. Ayachit, U.: The ParaView Guide: A Parallel Visualization Application. Kitware (2015)
 3. Bucki, M., Palombi, O., Bailet, M., Payan, Y.: Doppler Ultrasound Driven Biomechanical Model of the Brain for Intraoperative Brain-Shift Compensation: A Proof of Concept in Clinical Conditions. In: Soft Tissue Biomechanical Modeling for Computer Assisted Surgery, pp. 135–165. Springer (2012)
 4. Castellano-Smith, A.D., Hartkens, T., Schnabel, J.A., Hose, D.R., Liu, H., Hall, W.A.: Constructing Patient Specific Models for Correcting Intraoperative Brain Deformation. Medical Image Computing and Computer-Assisted Intervention - MICCAI 2001 pp. 1091–1098 (2001)
 5. Chen, I., Coffey, A.M., Ding, S., Dumpuri, P., Dawant, B.M., Thompson, R.C., Miga, M.I.: Intraoperative Brain Shift Compensation: Accounting for Dural Septa. IEEE Transcations on Biomedical Engineering **58**(3), 499 – 508 (2011)
 6. Courtecuisse, H., Allard, J., Kerfriden, P., Bordas, S.P.A., Cotin, S., Duriez, C.: Real-time simulation of contact and cutting of heterogeneous soft-tissues. Medical Image Analysis **18**, 394–410 (2014)
 7. Courtecuisse, H., Peterlik, I., Trivisonne, R., Duriez, C., Cotin, S.: Constraint-based simulation for non-rigid real-time registration. Medicine Meets Virtual Reality 21: NextMed/MMVR21 **196**, 76–82 (2014)
 8. Miga, M.I., Sun, K., Chen, I., Clements, L.W., Pheiffer, T.S., Simpson, A.L., Thompson, R.C.: Clinical evaluation of a model-updated image-guidance approach to brain shift compensation: experience in 16 cases. International journal of computer assisted radiology and surgery (2015)
 9. Miller, K., Lu, J.: On the prospect of patient-specific biomechanics without patient-specific properties of tissues. Journal of the mechanical behavior of biomedical materials **27**, 154–166 (2013)
10. Morin, F., Chabanas, M., Courtecuisse, H., Payan, Y.: Brain. In: to appear in Biomechanics of Living Organs: Hyperelastic Laws for Finite Element Modeling (2016)
11. Morin, F., Courtecuisse, H., Chabanas, M., Payan, Y.: Rest shape computation for highly deformable model of brain. Computer Methods in Biomechanics and Biomedical Engineering **18**(Sup1), 2006–2007 (2015)
12. Müller, M., Dorsey, J., McMillan, L., Jagnow, R., Cutler, B.: Stable real-time deformations. Proceedings of ACM SIGGRAPH Symposium on Computer Animation (SCA) pp. 49–54 (2002)
13. Nimsky, C., Ganslandt, O., Cerny, S., Hastreiter, P., Greiner, G., Fahlbush, R.: Quantification of, Visualization of, and Compensation for Brain Shift Using Intraoperative Magnetic Resonance Imaging. Neurosurgery **47**(5), 1070–1080 (2000)
14. Reinertsen, I., Descoteaux, M., Siddiqi, K., Collins, D.L.: Validation of vessel-based registration for correction of brain-shift. Medical Image Analysis **11**, 374–388 (2007)
15. Reinertsen, I., Lindseth, F., Askeland, C., Iversen, D.H., Unsgard, G.: Intra-operative correction of brain-shift. Acta Neurochirurgica **156**, 1301–1310 (2014)
16. Reinertsen, I., Lindseth, F., Unsgard, G., Collins, D.L.: Clinical validation of vessel-based registration for correction of brain-shift. Medical Image Analysis **11**, 673–684 (2007)
17. Rivaz, H., Collins, D.L.: Deformable registration of preoperative MR, pre-resection ultrasound, and post-resection ultrasound images of neurosurgery. International journal of computer assisted radiology and surgery **10**(7), 1017–1028 (2015)
18. Schiavone, P., Chassat, F., Boudou, T., Promayon, E., Valdivia, F., Payan, Y.: In vivo measurement of human brain elasticity using a light aspiration device. Medical Image Analysis **13**, 673–678 (2009)
19. Smith, S.M.: Fast Robust Automated Brain Extraction. Human Brain Mapping **17**(3), 143–155 (2002)
20. Sun, H., Roberts, D.W., Farid, H., Wu, Z., Hartov, A., Paulsen, K.D.: Cortical Surface Tracking Using a Stereoscopic Operating Microscope. Neurosurgery **56**(1), 86–97 (2005)
21. Vermandel, M., Betrouni, N., Taschner, C., Vasseur, C., Rousseau, J.: From MIP to MRA segmentation using fuzzy set theory. Computerized Medical Imaging and Graphics **31**, 128–140 (2007)

22. Vigneron, L.M., Noels, L., Warfield, S.K., Verly, J.G., Robe, P.A.: Serial FEM/XFEM-Based Update of Preoperative Brain Images Using Intraoperative MRI. International Journal of Biomedical Imaging **2012** (2012)
23. Wan, M., Liang, Z., Ke, Q., Hong, L., Bitter, I., Kaufman, A.: Automatic Centerline Extraction for Virtual Colonoscopy. IEEE Transactions on Medical Imaging **21**(12), 1450–1460 (2002)
24. Wittek, A., Hawkins, T., Miller, K.: On the unimportance of constitutive models in computing brain deformation for image-guided surgery. Biomechanics and modeling in mechanobiology **8**(1), 77–84 (2009)
25. Wittek, A., Miller, K., Kikinis, R., Warfield, S.K.: Patient-specific model of brain deformation: Application to medical image registration. Journal of Biomechanics **40**(4), 919–929 (2007)
26. Yushkevich, P.A., Piven, J., Cody Hazlett, H., Gimpel Smith, R., Ho, S., Gee, J.C., Gerig, G.: User-guided 3d active contour segmentation of anatomical structures: Significantly improved efficiency and reliability. NeuroImage **31**(3), 1116–1128 (2006)